PHYSICS AND CHEMISTRY OF SOLID STATE
V. 26, No. 4 (2025) pp. 766-773
Section: Physics

DOI: 10.15330/pcss.26.4.766-773

Vasyl Stefanyk Carpathian National University

ФІЗИКА І ХІМІЯ ТВЕРДОГО ТІЛА
Т. 26, № 4 (2025) С. 766-773
Фізико-математичні науки

PACS: 79.20.Hx

ISSN 1729-4428 (Print)
ISSN 2309-8589 (Online)

V. Kotsyubynsky[1], M. Cholewa[2], V. Kindrat[1], V. Boychuk[1], N. Mentynskyi[1], R. Abaszade[3,4,5,6], Y. Sukhorebskyi[7]

GEANT4 Study of Secondary Electron Emission in ZnO Nanorod Arrays under 10-100 MeV Oxygen Ion Irradiation

[1]*Vasyl Stefanyk Carpathian National University, Ivano-Frankivsk, Ukraine, volodymyr.kotsiubynskyi@cnu.edu.ua;*
[2]*Institute of Physics, College of Natural Sciences, University of Rzeszow, Rzeszow, Poland, mcholewa@ur.edu.pl;*
[3]*Azerbaijan University of Architecture and Construction, Baku, Azerbaijan, abaszada@gmail.com;*
[4]*Azerbaijan State Oil and Industry University, Baku, Azerbaijan;*
[5]*Turan International Research Institute, Baku, Azerbaijan;*
[6]*Tashkent State Technical University, Tashkent, Uzbekistan;*
[7]*Ivano-Frankivsk National Medical University, Ivano-Frankivsk, Ukraine*

Computational study of secondary electron emission (SEE) from ZnO nanorod arrays deposited on Au/Si_3N_4 substrates under irradiation with ^{16}O ions in the 10–100 MeV energy range was performed. Using a combination of SRIM and GEANT4 Monte Carlo simulations, the mechanisms of electronic stopping, electron excitation, and secondary electron yield (SEY) were systematically analyzed as functions of ion energy, nanorod radius, and substrate coverage. The results show that the dominant energy loss channel of oxygen ions in ZnO is electronic stopping, peaking at 20 MeV, which defines the optimal energy range for efficient SEE. ZnO nanorod arrays demonstrated significant advantages over continuous ZnO films, providing twice increase in SEY due to their high surface-to-volume ratio, anisotropic geometry, and local field enhancement at nanorod tips, which collectively improve both electron generation and escape. The study identified that nanorods with radii of 0.5–1.0 μm and moderate substrate coverage (35-50%) yield the best performance, achieving a favorable balance between interaction volume and electron escape probability. The findings highlight the importance of nanostructure engineering for tailoring SEE efficiency and provide predictive guidelines for the rational design of nanostructured emitters. In particular, ZnO nanorod arrays emerge as promising candidates for high-performance SEE-based detectors and diagnostic devices in plasma physics, ion-beam technologies, and space applications operating in the MeV energy regime. This work demonstrates the potential of advanced computational modeling in accelerating the development of optimized nanomaterials for electron emission and radiation detection.

Keywords: GEANT4, secondary electron emission, ZnO, secondary electron yield.

Received 14 June 2025; Accepted 18 November 2025.

Introduction

Secondary Electron Emission (SEE) has emerged as a critical technique for the detection of fast ions across a wide energy spectrum, ranging from keV to hundreds of MeV. Its high sensitivity, rapid response time, and adaptability to various ion types and energy levels make it indispensable in fields such as plasma diagnostics, particle accelerators, and space science. An advantage of SEE is its fast response time, on the order of 10^{-15} to 10^{-12} seconds, enabling real-time monitoring in high-energy environments. Secondary electron yield (SEY) varies significantly across different materials and is influenced by the energy of the primary ions. Study on transition metals reported maximum SEY values of 1.96 for titanium (Ti), 2.34 for zirconium (Zr), 1.72 for vanadium (V), and 2.32 for hafnium (Hf) [1]. Silicon exhibit SEY values up to 2, however, these the yield can be increased to 2.53 by nitrogen-doping levels change [2]. The mean escape depth

of SE, which influences SEY, has been found to vary among semiconductors, with calculated values showing significant scattering even within the same material, generally exhibiting SEY values in the range of 1 to 2 [3]. Wide-bandgap semiconductors (E_g>2.5-3.0 eV) exhibit SEY that are influenced by electronic structures and surface properties of emitters. Materials such as cubic boron nitride and aluminum nitride have been identified as effective emitters with SEY up to 4 and higher due to their surface and transport properties [4]. SEY of wide-bandgap semiconductors is linked to their electronic structure so the development in this field allow to increase SEE performance. The increasing surface area relative to volume causes the probability growth of SE escaping without recapture so the advances in nanostructures surface formation have opened new possibilities for SEY enhancing. Reduced dimensionality (e.g., 1D or 2D structures) minimizes scattering paths, enabling more electrons to retain sufficient energy to escape the surface. The design of nanostructures with specialized geometries– such as nanorods, nanowires, nanotubes, or porous surfaces– holds promise for optimizing electron emission angles and paths, thereby significantly enhancing SEE yield [5]. Surface engineering, including the application of coatings with low electron work function or the adjustment of surface potentials, can further reduce energy barriers for electron escape. Localized electric fields generated by nanostructured surfaces also contribute to improved SEE efficiency by accelerating and directing secondary electrons toward detectors. Fine-tuning material properties, such as bandgap, electron affinity, and surface charge, offers additional possibilities for optimizing performance. At the same time, the practical deployment of such advanced nanostructures requires careful consideration of technical feasibility, fabrication cost, and operational reliability.

Zinc oxide (ZnO) is a promising SEE material due its low electron affinity which promotes efficient electron escape from the surface in combination with wide bandgap (3.37 eV) which minimizes thermal excitation of electrons and ensures stable SEE performance at elevated temperatures [6]. Chemical stability of ZnO under various environmental conditions important for its durability and consistent performance as SEE emitter [7]. The versatility of ZnO in forming nanostructures (rods, wires, sheets) allows further enhances its SEE performance [8]. ZnO exhibits compatibility with advanced epitaxial growth techniques, enabling precise control over its electronic and surface properties to further improve SEE efficiency [9]. ZnO is also an economically viable choice, as it is abundant and cost-effective compared to other wide-bandgap. Key factors affecting SEE in ZnO nanorods comparatively to ZnO film is high surface-to-volume ratio increases the probability of electron scattering and emission. The improve transport properties due to their one-dimensional structure lead to efficient SEE, especially under high-energy excitation. The nanostructures surface typically have a higher density of surface defects, such as oxygen vacancies, which act as traps or recombination centers for electrons, potentially modifying SEE characteristics. Charge recombination efficiency is higher for solid films so, which may suppress SEE compared to nanorods. A non-homogeneous structure allows deeper penetration of the primary electron beam, increasing the likelihood of internal electron scattering and subsequent emission when denser material for solid films confines the beam interaction to a smaller depth, limiting SEE. Anisotropic geometry can cause angular variations in SEE, depending on the orientation of the nanorods relative to the primary electron beam when solid films generally show isotropic SEE due to their flat and uniform surface. The expected growth of SEY for ZnO nanorods comparatively to solid ZnO films is a result of increased surface area, geometric effects, and local electric field enhancement at sharp edges. Nanorods expectedly show broader energy distributions due to varied emission sites (tips, edges, and defects), while solid films exhibit narrower distributions. ZnO nanorods emission characteristics can be tuned by modifying their length, diameter, density, and surface chemistry. Computational modeling of SEE exploring material and geometric configurations allow enhance the efficiency of investigations with evaluating geometries and material properties. Among the available modeling platforms, GEANT4, a Monte Carlo-based simulation toolkit, offers significant prospects for advancing SEE studies [10]. GEANT4 is highly versatile and can simulate complex interactions of particles with matter, making it particularly suitable for predicting SEE yields under various ion types, energies, and material configurations. This study explores the simulation of SEE induced by the monochromatic fluxes of oxygen ions with energies in the range of 10-100 MeV. The general regularities of SE spectral distributions and SEY as functions of the ZnO nanorods diameters and their density on the Si3N4 substrate were established.

I. Experimental details

GEANT4 was employed to model the SEE properties of ZnO nanostructures under ^{16}O ion irradiation with exploration of SEY behavior as a function of nanorod dimensions, density, and target configurations, providing valuable insights into the optimization of emitter performance [11]. Target was defined as 30 x 30 μm silicon nitride (Si_3N_4) foil (1 μm thickness) covered with ultra-thin layers of gold (40 nm thickness). ZnO nanorods with a length of 5 μm and a radius in a range of 0.10, 0.25, 0.5, 1 and 1.25 (or 1.20) μm were regularly distributed on the Si_3N_4/Au substrate with a different pitch distances. Totally 6 variants of nanorod densities were analyzed – 0,4 ,100, 400, 625 and 900 nanorods per target substrate with the area of 900 μm2. The relative areas of nanorods cross-section were 0 (empty Si_3N_4/Au), 12.6, 35.0, 50.2, 78.5 and 100 (ZnO film of 5 μm thickness) %, respectively.

The targets were irradiated with ^{16}O beam (total number of primary particles is 5000, starting energies of primary particles are 10, 20, 30, 40, 50, 70 and 100 MeV or 0.625, 1.25, 1.875, 2.5, 3.125, 4.375 and 6.25 MeV/u; initial particles velocities are directed normally to Si_3N_4/Au substrate plane. ^{16}O ions were generated from random points of virtual 30×30 μm plane located parallel to Si_3N_4/Au substrate “above” ZnO nanorod arrays. SEE processes were traced and spectra of SE were obtained. Only SE that reached the detectors were analyzed

statistically. The detectors were two infinite planes parallel to the substrate, located in front of and behind the substrate. The idea was to determine the dependence of the SEY on the nanorods radius and density on the substrate when irradiated with oxygen ions in the energy range. Physics List Used at simulation procedures: G4EmStandardPhysics_option4; G4DecayPhysics; G4IonPhysics; G4EmLivermorePhy–sics. The Stopping and Range of Ions in Matter (SRIM) software was used to simulate the interaction of ^{16}O ions with target with modeling of ion penetration and energy deposition using Monte Carlo algorithms suitable for real-world experimental setups [12, 13].

II. Results and Discussion

SRIM calculation of ^{16}O ions stopping powers in ZnO /Au /Si_3N_4 multilayered target demonstrate that the main mechanism of energy loss is inelastic collisions (about 99.7 % of total energy loss) with excitation of electronic of the target's atoms. The probability that a primary ^{16}O ion will leave ZnO nanorod under the experimental condition is neglected small. The distribution of energy transferred to the target electrons during stopping of ^{16}O ions with different energies is shown in the Fig.1a. At the lowest energy considered (10 MeV), the ions are fully stopped within the ZnO nanorods, resulting in a concentrated energy deposition profile inside the oxide layer. In contrast, ions with higher initial energies traverse the entire multilayer structure, leading to a broader and less localized energy deposition. This transition indicates that the confinement of energy within ZnO is strongly dependent on the incident energy, with low-energy projectiles maximizing electronic excitations inside the nanostructured emitter, whereas higher-energy ions deposit part of their energy deeper into the supporting layers or escape the system altogether.

Figure 1b quantifies the electronic stopping power of ^{16}O ions in the multilayer target as a function of ion energy. The maximum electronic energy loss is observed for 20 MeV ions, reaching 13.7 MeV/μm, after which a monotonic decrease occurs with increasing projectile energy. This behavior reflects the Bethe–Bloch dependence, where stopping power first rises with increasing energy until it reaches a peak in the so-called Bragg maximum region, followed by a gradual decline as the ions become relativistic. The dominance of inelastic collisions (> 99% of the total energy loss) underlines the efficiency of ^{16}O ions in exciting the electronic subsystem of ZnO, thus generating conditions favorable for SEE. The maximum electronic excitation are in the 15–30 MeV energy window for ZnO nanostructures. At higher energies the reduced stopping power and deeper penetration lower the fraction of energy available for electron production in the nanorod layer, which may limit the SEE.

EE from ZnO/Au/Si_3N_4 under ^{16}O ion irradiation in the used energy range (10-100 MeV) is a complex process influenced by the material's electronic structure, ion energy, and surface properties. The energy deposited by the ion beam excites electrons in the conduction band and valence band, creating a high-density electron-hole plasma consisting of primary energetic electrons (delta electrons) and secondary low-energy electrons. The primary electrons are generated by direct ionization and possess sufficient energy to excite additional electrons via collisions, amplifying the electron emission process. ZnO as wide-bandgap materials exhibit strong resistance to thermal effects, allowing more efficient transfer of ion energy to electronic excitations rather than phonons. The energy spectra of electrons emitted from ZnO include contributions both from primary δ-electrons and SE. The spectra of electrons directly after excitation (before emission) involves understanding the energy distribution of electrons generated by the ionization process within ZnO (Fig. 2). These electrons are a mix of high-energy electrons ejected directly by the interaction of the incident ion with the target atoms and secondary electrons generated from subsequent collisions of primary electrons within the material.

The intense peak at 0.265 keV as well as a long tail with energies up to 10-15 keV observed for both bulk and nanostructured ZnO coating correspond to δ-electrons. This suggestion agrees with conclusions of Bethe-Bloch stopping theory. Three distinct morphologies were analyzed: a solid ZnO film of 5 μm thickness, an array of ZnO nanorods with 1 μm radius covering 50.2% of the substrate, and a nanorod array of identical radius and thickness but with lower coverage (12.6%). In all cases,

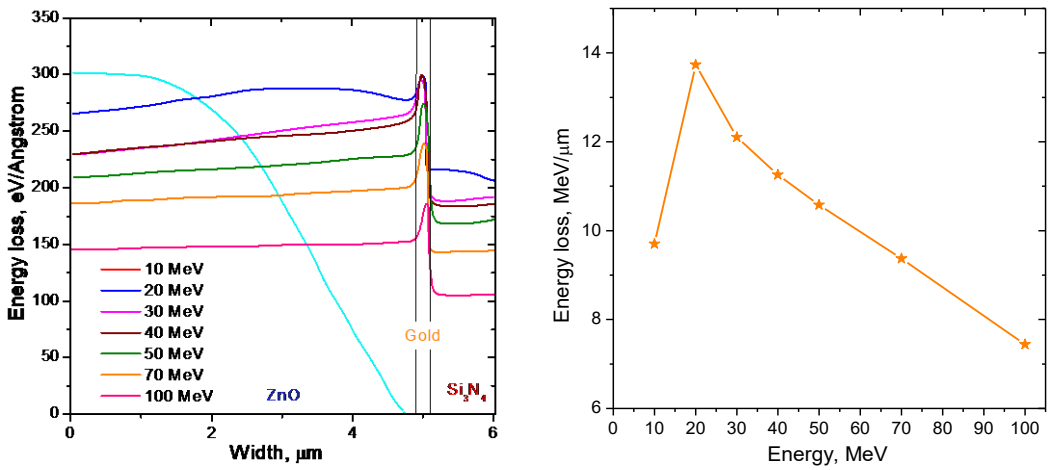

Fig.1. (a) SRIM estimates of an energy deposition during stopping of 16O ions with different energies in ZnO/Au/Si3N4 structure and (b) electronic energy loss of ^{16}O ions as a function of its energies.

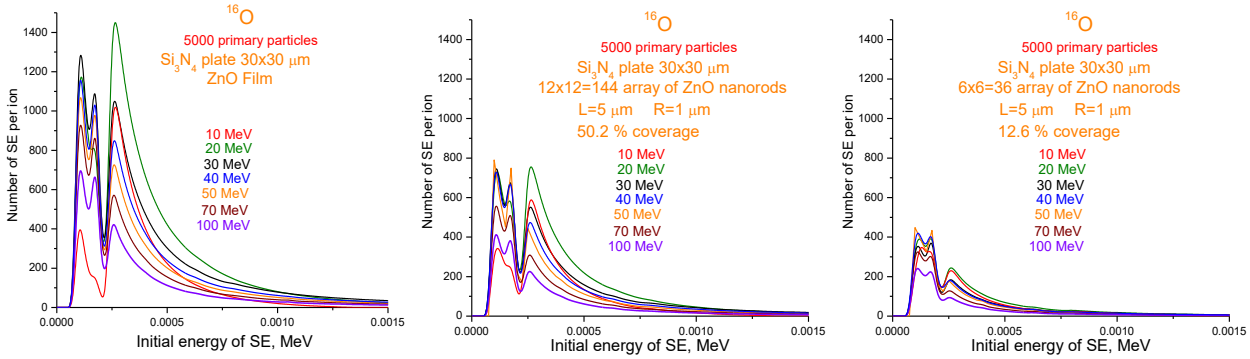

Fig. 2. GEANT4 simulated spectra of initial energy of electrons (energy at the moment of excitation by fast ion or primary electron) induced by 16O ions with energy in a range of 10-100 MeV from ZnO/Au/Si_3N_4 target with different morphology: (a) solid ZnO film with the thickness of 5 μm, (b) array of ZnO nanorod with radius of 1 μm, thickness of 5 μm and coverage of 50.2 % of substrate, (c) array of ZnO nanorod with radius of 1 μm, thickness of 5 μm and coverage of 12.6 % of substrate.

the spectra consist of two characteristic features: an intense peak at 0.265 keV and an extended tail reaching up to 10–15 keV. The peak corresponds to the abundant generation of low-energy secondary electrons, while the long tail arises from higher-energy δ-electrons produced during ionization cascades. The coexistence of both components reflects the complex interplay between direct ionization by the projectile and subsequent electron–electron scattering within the material, in agreement with the Bethe–Bloch stopping mechanism.

The morphology of the ZnO significantly influences the electron distribution. The dense nanorod array (50.2% coverage) exhibits a broader energy spectrum compared to the solid ZnO film, indicating enhanced electron escape channels provided by the anisotropic geometry and local electric field effects at the nanorod tips.

Conversely, the sparse array (12.6% coverage) produces fewer low-energy electrons but retains relatively higher contributions from δ-electrons, suggesting that reduced interaction volume decreases overall excitation but allows a higher fraction of energetic carriers to escape without scattering losses.

Figure 3 presents the simulated dependence of SEY on the incident energy of ^{16}O ions for various ZnO target morphologies. Several clear trends emerge. SEY exhibits a non-monotonic dependence on ion energy, with a pronounced maximum in the 20–30 MeV range. This correlates with the peak in electronic stopping power (Fig. 1b), where energy transfer from ions to the electronic subsystem of ZnO is most efficient. At 10 MeV, although ions are fully stopped within the nanorod layer (Fig. 1a), the reduced penetration depth confines excitation to a small interaction volume, which limits the number of secondary electrons able to reach the surface. At higher energies (>50 MeV), the electronic stopping decreases steadily, lowering the excitation density within ZnO and thereby reducing SEY. This behavior is consistent with the Bethe–Bloch framework for ion–solid interactions and has been observed in other dielectric and wide-bandgap systems. Nanostructured ZnO surfaces clearly outperform flat films across the entire energy range. Arrays of nanorods provide enhanced electron escape channels due to their high surface-to-volume ratio, anisotropic geometry, and localized electric field effects at the rod tips. This leads to a broader and higher SEY compared with solid ZnO films, where electron recombination within the bulk strongly suppresses emission.

For intermediate energies near the stopping maximum, arrays with moderate coverage (≈50%) and radii of 0.5–1.0 μm deliver the highest yields, striking a balance between sufficient interaction volume and efficient electron escape. At small radii (< 0.25 μm), although the surface area is large, the reduced interaction volume limits the number of generated electrons. Conversely, at high coverage approaching 100% (solid film), recombination losses dominate, and SEY decreases compared with optimized nanorod arrays. This behavior highlights the critical role of geometric tuning in maximizing detector performance.

Figure 3b illustrates the dependence of secondary electron yield (SEY) on the radius of ZnO nanorods for various substrate coverages and incident ion energies. The results clearly demonstrate that nanorod geometry is a critical determinant of SEE efficiency. A general trend is observed in which SEY increases with nanorod radius up to an optimal range of approximately 0.5–1.0 μm, followed by saturation or a slight decline for larger radii. This non-linear dependence can be rationalized by considering the interplay between interaction volume and surface escape probability. At small radii (< 0.25 μm), the high surface-to-volume ratio enhances electron escape pathways, but the limited interaction volume reduces the absolute number of generated secondary electrons. As the radius increases, a larger target volume per nanorod enhances electron production, while the retention of a relatively high surface-to-volume ratio ensures efficient emission. However, once the rods become sufficiently thick (>1.0 μm), the increased recombination probability within the interior of the nanorods outweighs the benefits of a larger interaction volume, leading to reduced SEY.

The influence of substrate coverage is equally significant. At moderate coverage levels (35–50%), the SEY is maximized, as this configuration provides a balanced combination of electron generation and escape efficiency. Sparse arrays (coverage ~12.6%) yield lower SEY due to insufficient interaction cross-section, while extremely dense arrays or continuous films (100% coverage) exhibit suppressed yields because of enhanced recombination losses and isotropic emission geometry. This behavior underlines the importance of avoiding both

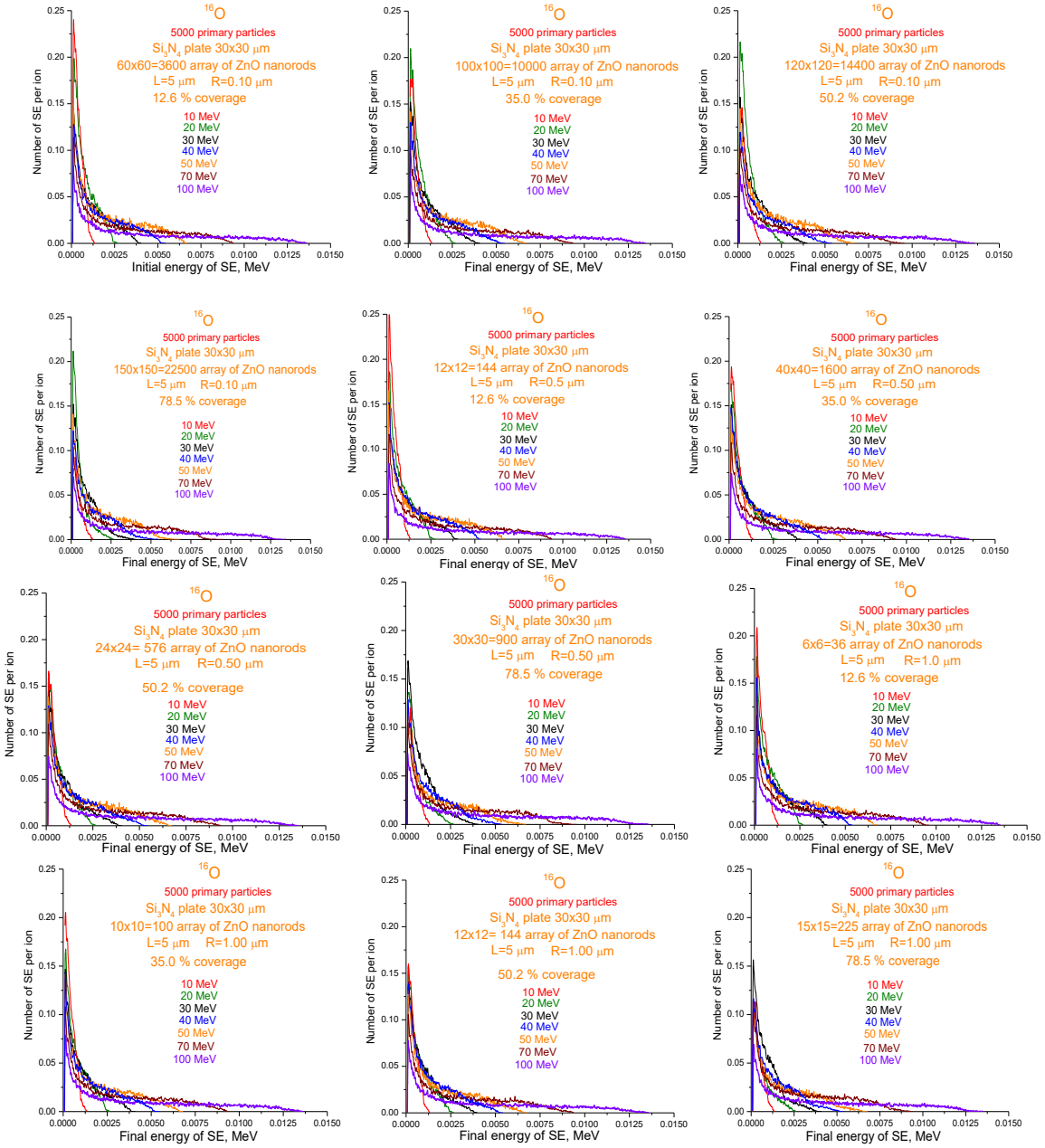

Fig. 3. GEANT4 simulated spectra of detected electrons (energies of electrons that reached the detectors).

under- and over-saturation of nanostructure density. The ion energy further modulates these trends. At intermediate energies near the stopping power maximum (20-30 MeV), the sensitivity of SEY to nanorod radius is strongest, reflecting the efficient coupling of energy deposition with optimal nanorod dimensions. At higher energies (> 50 MeV), the overall SEY decreases due to reduced stopping, but the relative differences between radii remain discernible. At low energies (10 MeV), confinement of the ion path within the rods reduces the impact of geometric variation, since nearly all of the energy is absorbed within a limited depth regardless of radius.

Figure 5 presents the simulated dependence of SEY on the energy of ^{16}O ions for ZnO targets of varying nanorod radii (0.1–1.25 μm) and substrate coverages (12.6%, 35.0%, 50.2%, 78.5%), compared to a solid ZnO film. Across all radii and coverages, SEY demonstrates a non-monotonic behavior with a pronounced maximum in the intermediate energy range of 20-40 MeV. This is consistent with the stopping power profile of oxygen ions (Fig. 1b), where energy transfer to the electronic subsystem peaks in this region. At low energies (10–20 MeV), although ions deposit most of their energy within the ZnO layer, the shallow penetration depth limits the generation of escaping secondaries. At high energies (> 50 MeV) reduced electronic stopping lowers the excitation density, leading to a gradual decline in SEY. For all ion energies, nanostructured ZnO surfaces significantly outperform bulk films. Arrays of nanorods exhibit enhanced SEY due to their high surface-to-volume ratio, anisotropic geometry, and localized electric field effects, which increase the probability of electron escape. This advantage is particularly pronounced in the 20–40 MeV energy window, where SEY values are nearly doubled compared to bulk. For R = 0.1 μm SEY is enhanced compared to bulk but limited by the small interaction volume, leading to lower overall electron production.

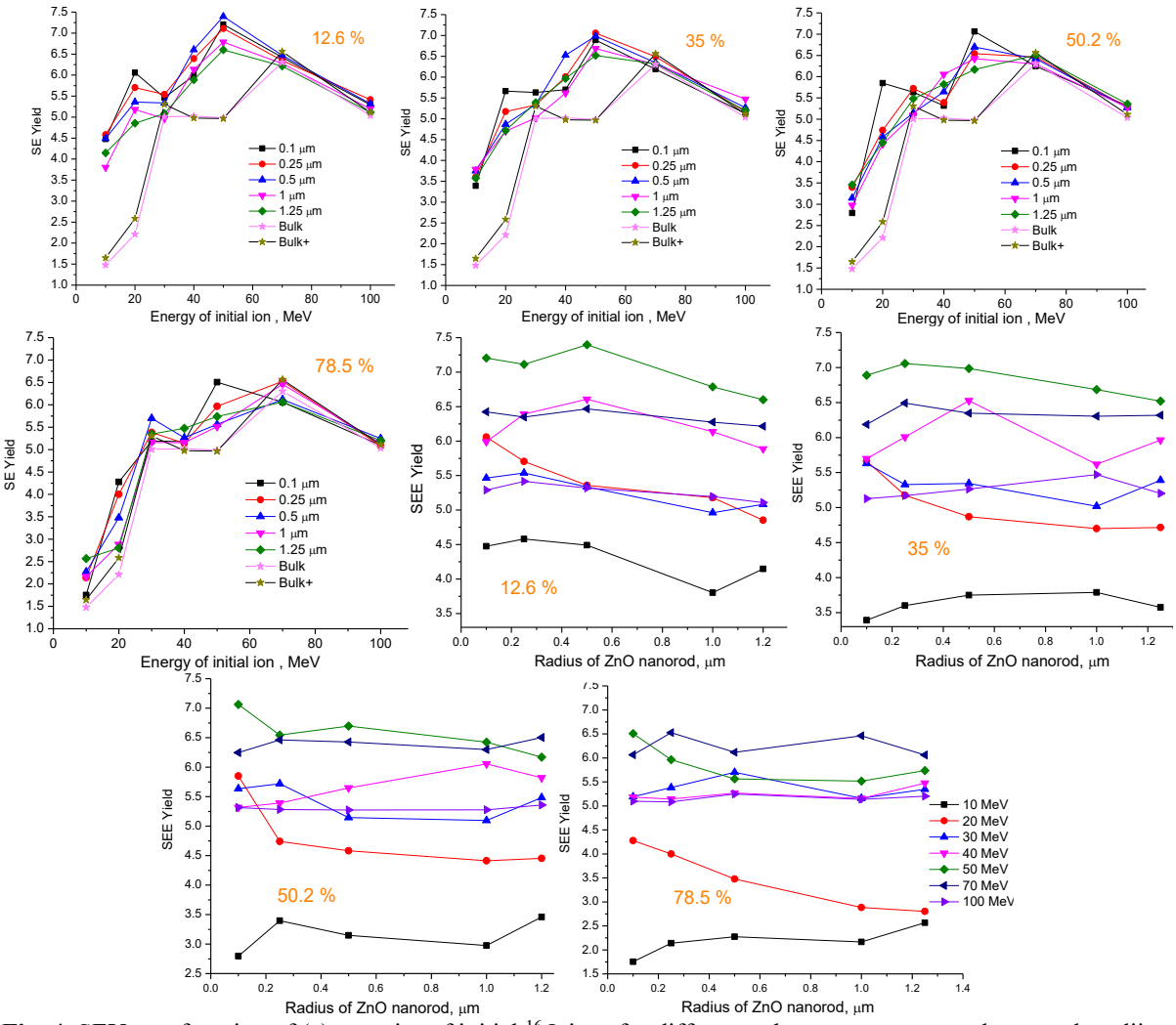

Fig. 4. SEY as a function of (a) energies of initial ^{16}O ions for different substrate coverage and nanorods radii and (b) nanorods radii for different substrate coverage and energies of initial ^{16}O ions.

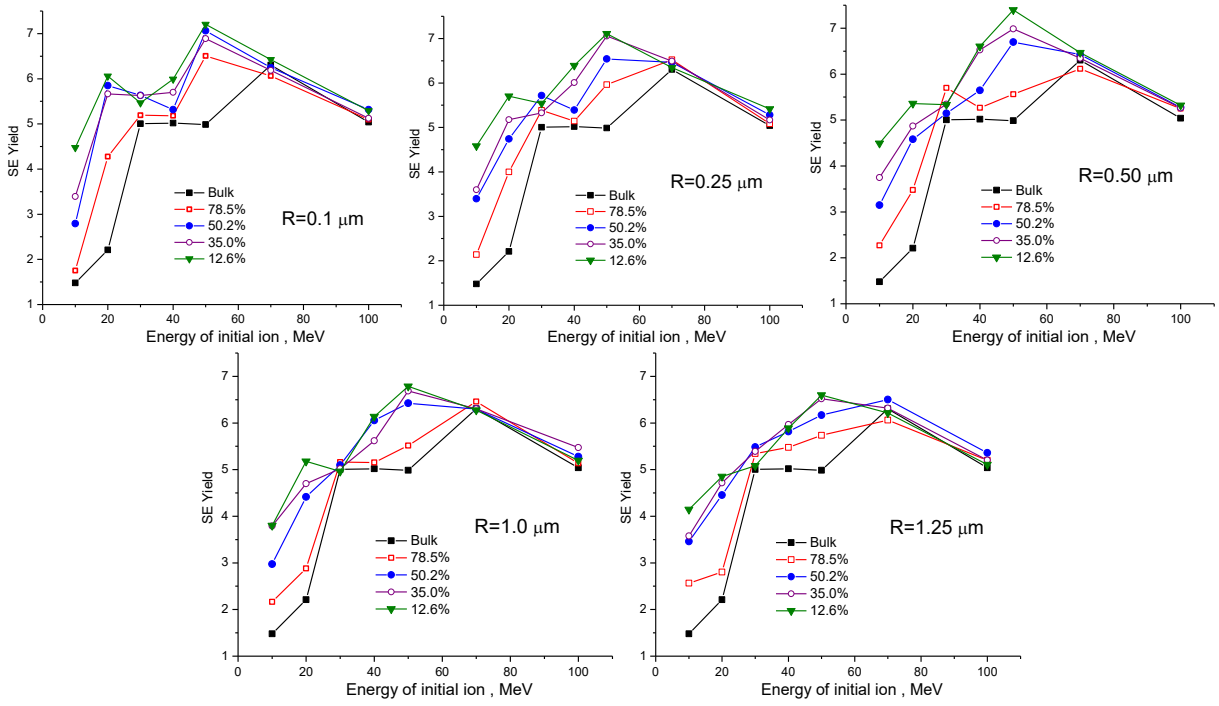

Fig. 5. Dependence of the secondary electron yield (SEY) on the energy of incident ^16O ions (10–100 MeV) for ZnO nanorod arrays with radii of 0.1, 0.25, 0.5, 1.0, and 1.25 μm. Results are shown for different substrate coverages (12.6%, 35.0%, 50.2%, 78.5%) in comparison with a bulk ZnO film (black line).

As the radius increases to 0.25-1.0 μm SEY rises reaching values where interaction volume is sufficient to generate large numbers of electrons while surface-to-volume ratio remains favorable for escape. At R=1.25 μm, SEY begins to saturate or slightly decline, reflecting increased recombination losses in thicker nanorods. Thus, the optimal geometry lies in the intermediate radius range of 0.5–1.0 μm. Sparse arrays (12.6% coverage) yield relatively high SEY at certain energies due to reduced scattering pathways for δ-electrons, but overall electron generation is limited by the small effective cross-section. Moderate coverages (35–50%) consistently provide the highest SEY, balancing sufficient electron production with efficient escape. Dense arrays (78.5%) approach the behavior of a continuous film, where recombination and isotropic emission suppress the enhancement effect.

Conclusions

This study used GEANT4 and SRIM simulations to investigate the mechanisms of SEE from ZnO nanorod arrays on Au/Si_3N_4 substrates under irradiation with ^{16}O ions in the 10-100 MeV range. The results revealed that the dominant energy loss channel of oxygen ions in ZnO is electronic stopping (>99%), which efficiently excites the electronic subsystem of the material. The maximum electronic stopping power was observed at 20 MeV, corresponding to the Bragg peak region, where electron excitation and subsequent SEE processes are most effective. Analysis of electron energy spectra demonstrated the coexistence of abundant low-energy secondaries and higher-energy δ-electrons, with nanostructured ZnO exhibiting broader and more intense distributions compared to flat films. This enhancement arises from the increased surface-to-volume ratio, anisotropic geometry, and local field effects of nanorods, which collectively facilitate electron escape. The dependence of secondary electron yield (SEY) on ion energy, nanorod radius, and substrate coverage confirmed that geometric optimization plays a decisive role in maximizing emission.

SEY was found to peak in the intermediate energy range of 20-40 MeV, consistent with the maximum in electronic stopping power.

Nanostructured targets consistently outperformed bulk ZnO across all energies, with the most favorable yields achieved for nanorods with radii of 0.5–1.0 μm and substrate coverages of 35–50%. Sparse arrays, although offering efficient escape for energetic electrons, generated fewer overall secondaries due to limited interaction cross-section, while densely packed arrays approached bulk-like behavior with enhanced recombination losses. Very thin rods (< 0.25 μm) produced limited yields due to insufficient interaction volume, whereas thick rods (> 1.0 μm) exhibited reduced efficiency from increased recombination.

Kotsyubynsky V.O. – Professor, Doctor of Sciences;
Cholewa M. – Professor, Doctor of Sciences;
Kindrat V. – PhD student;
Boychuk V.M. – Professor, Doctor of Sciences;
Mentynskyi N. – PhD student;
Abaszade R. – PhD, Associate Professor;
Sukhorebskyi Y. – PhD, Associate Professor.

[1] S. Wang, O. B. Malyshev, R. Valizadeh, E. A. Seddon, M. D Cropper *The secondary electron yield from transition metals,* Proc. of IPAC2014, Dresden, Germany, 2403 (2014); https://doi.org/10.18429/JACoW-IPAC2014-WEPME057.
[2] Y. Zhao, X. Meng, S. Peng, G. Miao, Y. Gao, B. Peng, Z. Hu *Physical mechanism of secondary-electron emission in Si wafers,* Chinese Physics B, 33(4), 047901 (2024); https://doi.org/10.1088/1674-1056/ad1175.
[3] A. G. Xie, S. R. Xiao, H. Y. Wu *Mean escape depth of secondary electrons emitted from semiconductors and insulators*. Indian Journal of Physics, 87, 1093 (2013); https://doi.org/10.1007/s12648-013-0355-8.
[4] J. E. Yater *Secondary electron emission and vacuum electronics,* Journal of Applied Physics, 133(5) (2023); https://doi.org/10.1063/5.0130972.
[5] M. Cholewa, A. Grędysa, A. Pozaruk, T. Osipowicz, J. A. van Kan, Y. X. Dou, P. Boutachkov *Investigating the Secondary Electron Emission of Nanomaterials Induced by a High-Resolution Proton Beam,* physica status solidi (b), 259(4), 2100445 (2022); https://doi.org/10.1002/pssb.202100445f.
[6] Zhong Lin Wang *Zinc oxide nanostructures: growth, properties and applications*, Journal of Physics: Condensed matter 16.25, R829 (2004); https://doi.org/10.1088/0953-8984/16/25/R01.
[7] Ü. Özgür, Y. I. Alivov, C. Liu, A. Teke, M. A. Reshchikov, S. Doğan, A. H. Morkoç. *A comprehensive review of ZnO materials and devices,* Journal of Applied Physics, *98*(4) (2005); https://doi.org/10.1063/1.1992666.
[8] A. Janotti, C. G. Van de Walle *Fundamentals of zinc oxide as a semiconductor,* Reports on progress in Physics, 72(12), 126501 (2009) https://doi.org/10.1088/0034-4885/72/12/126501.
[9] M. T. Noman, N. Amor, M. Petru *Synthesis and applications of ZnO nanostructures (ZONSs): A review,* Critical Reviews in Solid State and Materials Sciences, *47*(2), 99 (2022); https://doi.org/10.1080/10408436.2021.1886041.
[10] J. L. Gomez, O. Tigli. *Zinc oxide nanostructures: from growth to application,* Journal of Materials Science 48 612 (2013); https://doi.org/10.1007/s10853-012-6938-5.
[11] J. Allison, K. Amako, J. Apostolakis, P. Arce, M. Asai, T. Aso, H. Yoshida *Recent developments in Geant4* Nuclear instruments and methods in physics research section A: Accelerators, Spectrometers, Detectors and Associated Equipment, 835, 186 (2016); https://doi.org/10.1016/j.nima.2016.06.125.
[12] J. F. Ziegler, M. D. Ziegler, J. P. Biersack *SRIM– The stopping and range of ions in matter* Nuclear Instruments and Methods in Physics Research Section B: Beam Interactions with Materials and Atoms, 268(11-12), 1818 (2010); https://doi.org/10.1016/j.nimb.2010.02.091.

[13] I. Fodchuk, A. Kotsyubynsky, A. Velychkovych, I. Hutsuliak, V. Boychuk, V. Kotsyubynsky, L. Ropyak *The Effect of Ne^+ Ion Implantation on the Crystal, Magnetic, and Domain Structures of Yttrium Iron Garnet Films*. *Crystals*, *12*(10), 1485 (2022); https://doi.org/10.3390/cryst12101485.

В. Коцюбинський[1], М. Холева[2], В. Кіндрат[1], В. Бойчук[1], Н. Ментинський[1], Р.Абасзаде[3,4,5,6], Ю.Сухоребський[7]

Індукована опроміненням іонами оксигену (E=10-100 МеВ) вторинна емісія електронів з масивів нанотрубок ZnO: GEANT4 моделюваня

[1]Карпатський національний університет імені Василя Стефаника, Івано-Франківськ, Україна volodymyr.kotsiubynskyi@cnu.edu.ua;
[2]Інститут фізики, Жешівський Університет, Жешув, Польща, mcholewa@ur.edu.pl;
[3]Азербайджанський університет архітектури та будівництва, Баку, Азербайджан, abaszada@gmail.com;
[4]Азербайджанський державний нафтовий і промисловий університет, Баку, Азербайджан;
[5]Міжнародний науково-дослідний інститут «Туран», Баку, Азербайджан;
[6]Ташкентський державний технічний університет, Ташкент, Узбекистан;
[7]Івано-Франківський національний медичний університет, Івано-Франківськ, Україна

Було проведено обчислювальне дослідження вторинної емісії електронів з масивів наностержнів ZnO, нанесених на підкладки Au/Si_3N_4, під дією іонів оксигену в діапазоні енергій 10-100 МеВ. За допомогою комбінації моделювання SRIM і GEANT4 Monte Carlo було систематично проаналізовано механізми гальмування, збудження і вторинної емісії електронів як функції енергії іонів, радіуса наностержнів та щільності їх розміщення на підкладці. Результати показують, що домінуючим механізмом втрати енергії іонів кисню в ZnO є електронне гальмування, яке досягає піку при 20 МеВ, що визначає оптимальний діапазон енергій для ефективного емісії. Масиви наностержнів ZnO продемонстрували переваги над плівками ZnO, забезпечуючи майже двократне збільшення виходу вторинних електронів завдяки анізотропній геометрії та локальному посиленню електричних полів на краях наностержнів, що покращує як генерацію, так і емісію електронів. Дослідження показало, що наностержні з радіусом 0,5–1,0 мкм і середнім покриттям підкладки (35–50%) забезпечують оптимальні характеристики емісії. Отримані дані свідчать про важливість інженерії наноструктур для регулювання ефективності вторинної електронної емісії та можуть служити базою для проектування наноструктурних емітерів. Показано, що масиви наностержнів ZnO є перспективними для створення детекторів швидких йонів та діагностичних пристроїв у плазмовій фізиці та космічних застосуваннях. Продемонстровано потенціал комп'ютерного моделювання для прискорення розробки наноструктурованих емітерів електронів.

Ключові слова: GEANT4, вторинна емісія електронів, ZnO, вихід вторинних електронів.